Two-Stage Carrier Frequency Offset Estimation Using Eigenvalue and Scattering Coefficient b in Inverse Scattering Transform

Taisuke Chino, Takumi Motomura, *Graduate Student Member, IEEE*, Takaya Maeda, Akihiro Maruta, *Member, IEEE*, and Ken Mishina, *Member, IEEE*

***Abstract*—Inverse scattering transform (IST)-based transmission is one of the known approaches to overcome the Kerr nonlinearity limit in optical fiber communication systems. IST is known as Nonlinear Fourier transform (NFT) in optical fiber communications. However, the effect of carrier frequency offset (CFO) in digitally coherent receivers induces scattering data shifts in IST. Therefore, fine CFO estimation and compensation are required particularly for multilevel modulation based on IST. This paper proposes a two-stage CFO estimation method using eigenvalue and scattering coefficient b in IST. Numerical simulations and experiments investigate the estimation accuracy of the proposed method. The proposed method provides a high-accuracy estimation and covers a wide range of the CFO. An estimation accuracy of less than 10 kHz error is achieved under pulse period (25.6 ns) and sampling rate (10 GSa/s). Furthermore, we demonstrate that the proposed method is valid even for two-soliton solutions with a multipeak spectrum.**

***Index Terms*—Carrier frequency offset, eigenvalue modulation, optical soliton, *b*-modulation.**

I. Introduction

INVERSE scattering transform (IST) [1]-based transmission has been studied for one of approaches for overcoming the Kerr nonlinearity limit in optical fiber communication systems. IST is commonly known as the nonlinear Fourier transform (NFT) in optical fiber communications [2] Eigenvalues of eigenvalue equations associated with the nonlinear Schrödinger equation (NLSE) are invariant during optical fiber propagation, although waveform and spectrum change due to the effects of fiber dispersion and nonlinearity. The scattering coefficient b and norming constant in IST remain unaffected by nonlinear distortion because they linearly evolve during optical fiber transmission. To increase transmission capacity, various NFT-based transmission methods using multilevel and multi-eigenvalue have been proposed; for example, quadrature phase shift keying (QPSK) and 16-quadrature amplitude modulation (QAM) of the coefficient b [3] and 4096-ary signal transmission based on on–off encoding of 12 eigenvalues [4].

IST-based transmissions use a generic digital coherent receiver to obtain the complex envelop amplitude of an optical signal and detect scattering data including eigenvalues, norming constants, and scattering coefficients. Carrier frequency offset (CFO) estimation is necessary to estimate and compensate for wavelength mismatch between carrier signal and local oscillator (LO). The mismatch can reach approximately $\pm$ 5 GHz with a micro-integrable tunable laser assembly (ITLA) [5], [6], [7] because CFO induces shifts of eigenvalues and rotations of scattering coefficients, resulting in symbol errors.

Recently, several CFO estimation methods have been proposed, such as an algorithm using periodogram [8] in the frequency domain (FD) [9], [10], [11]. A study [9] has determined peak frequency using the periodogram method for the quadrature of a QAM signal to achieve highly accurate pilotless estimations. Another study has proposed CFO estimation without removing the modulated data phase [10]. Researchers have estimated a wide and accurate CFO estimation method without removing the modulation component by inserting a digital pilot and determining the position of the digital pilot in the spectrum [11]. However, the periodogram-based CFO estimation method requires a large number of samples to achieve high accuracy owing to the resolution.

Contrarily, several CFO estimation methods based on IST have been proposed [12], [13]. In our previous study, we proposed an eigenvalue-based estimation [12], which covered a wide CFO range of $\pm$5 GHz; however, the estimation accuracy was approximately 1 MHz. Although the method based on coefficient b can potentially achieve high accuracy, the estimation range is limited [13]. Additionally, the coefficient b-based method had not been experimentally validated. An estimation method that simultaneously achieves a high accuracy estimation and covers a wide range CFO for high multilevel eigenvalue modulation was yet to be studied. In our recent study [14], we proposed a two-stage CFO estimation method that combines the eigenvalue-based and coefficient b-based estimation methods. In the proposed method, CFO is roughly estimated in the eigenvalue domain at the first stage. In the second stage, fine

Received 5 November 2024; revised 24 March 2025 and 26 April 2025; accepted 28 April 2025. Date of publication 30 April 2025; date of current version 16 July 2025. This work was supported in part by the National Institute of Information and Communications Technology (NICT), Japan, under Project J012368C08401, in part by the KDDI Foundation, Japan, and in part by Shimadzu Science Foundation, Japan. *(Corresponding author: Ken Mishina.)*

The authors are with the Graduate School of Engineering, Osaka University, Suita, Osaka 565-0871, Japan (e-mail: chino22@pn.comm.eng.osaka-u.ac.jp; motomura22@pn.comm.eng.osaka-u.ac.jp; maeda@pn.comm.eng.osaka-u.ac.jp; maruta@comm.eng.osaka-u.ac.jp; mishina@comm.eng.osaka-u.ac.jp).

Color versions of one or more figures in this article are available at https://doi.org/10.1109/JLT.2025.3565884.

Digital Object Identifier 10.1109/JLT.2025.3565884

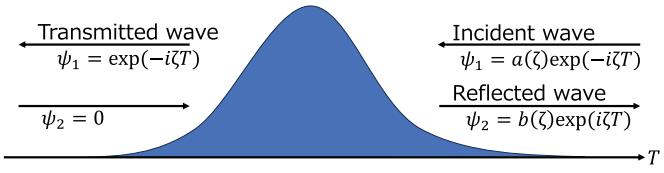

Fig. 1. Direct scattering problem.

CFO estimation is performed using the coefficient b. A pilotless CFO estimation method improving the two stage method has been demonstrated by another research group [15]. However, the detailed characteristics of the two-stage estimation method are was yet to be studied.

In this paper, as an extension of our previous study [14], we examine the two-stage CFO estimation method in detail and further investigate generalized characteristics, including the effects of time window size, sampling rate, eigenvalue, the number of pulses, and noise. Simulation results show that the estimation error is limited by time window size and sampling rate. However, by using appropriate parameters, a fine estimation of 10 kHz covering a wide range of CFO of ± 5 GHz can be achieved in the simulation. Furthermore, the proposed method provides highly accurate estimation even for two soliton solutions. Through experiments, we demonstrate that a fine estimation accuracy below 10 kHz can be achieved using the proposed method.

In the following, we will clarify the differences between the current and previous studies [12], [13], [14], [15]. Previous studies [12] and [13] utilize the eigenvalue and scattering coefficient b for CFO estimation, respectively. However, these methods had issues of low estimation accuracy and a limited estimation range, respectively. This study achieves a high estimation accuracy and a wide estimation range in the two-stage estimation by combining the eigenvalue and scattering b-base methods. The concept was proposed in our previous work [14]; however, the detailed analysis had not yet been discussed. The modifications and improvements to [14] are summarized as follows:

- A detailed explanation of the theory and methodology for the proposed CFO estimation method is provided.
- Several characteristics of the proposed method are investigated, including the dependency of the number of pulses, eigenvalue dependency, and noise dependency
- The application of the proposed method to two-soliton solutions is discussed, with the aim of applying it to b-modulation
- Discussion of the feasibility of the pilotless estimation and the computational complexity.

A similar two-stage estimation using the eigenvalue and scattering coefficient b was demonstrated by [15] after our proposal [14]; however, the detailed characteristics and analyses of the two-stage CFO estimation method, such as the dependencies of some conditions on estimation accuracy described above, were not discussed.

The rest of the paper is organized as follows. Section II introduces IST and CFO estimation methods using eigenvalues and scattering coefficient b. Section III discusses numerical simulation results. Section IV discusses the experimental results to demonstrate the feasibility of the proposed method. Finally, Section V concludes the study.

II. IST-Based CFO Estimation Method

A. NLSE and IST

The behavior of the complex envelope amplitude of a light wave propagating in an optical fiber is described by [16]:

$$i\frac{\partial E}{\partial z} - \frac{\beta_2}{2}\frac{\partial^2 E}{\partial t^2} + \gamma|E|^2 E = -i\alpha E, \tag{1}$$

where $z, t, E(z,t), \beta_2, \gamma$, and α are the propagation length, time, complex envelope amplitude of the electric field, group velocity dispersion, nonlinear parameter, and fiber loss, respectively. In (1), we assumed that the third-order dispersion and Raman scattering effects were negligible for a pulse width >1 ps. Furthermore, a scalar propagation of single-polarization component is considered. The parameters are normalized using reference time t_0. We consider a transmission channel where the amplifier spacing is sufficiently shorter than the dispersion length $t_0^2/|\beta_2|$ in the anomalous dispersion regime [17]. Further, (1) can be transformed into the standard form of the normalized NLSE as

$$i\frac{\partial u}{\partial Z} + \frac{1}{2}\frac{\partial^2 u}{\partial T^2} + |u|^2 u = 0, \tag{2}$$

where Z, T, and $u(Z,T)$ are the normalized propagation length, time, and electric field, respectively. Eigenvalue equation associated to (2) is expressed as

$$\begin{cases} \frac{\partial \phi_1}{\partial T} = -i\zeta\phi_1 + iu\phi_2 \\ \frac{\partial \phi_2}{\partial T} = iu^*\phi_1 + i\zeta\phi_2 \end{cases} \tag{3}$$

where ζ and $\phi_l (l = 1, 2)$ are complex eigenvalue and eigen function, respectively. Provided u satisfies (2), the eigenvalue ζ is invariant with respect to Z.

We consider a scattering problem expressed in (3), where $u(Z,T)$ is the potential [1]. An overview of the direct scattering problem is shown in Fig. 1. The problem implies that the reflected and transmitted waves are derived for incident waves from $T = \infty$. We assume that $u(0,T)$ satisfies the boundary condition of $u = 0$ for $|T| \to \infty$. For a real eigenvalue $\zeta = \xi$, we define the Jost function, ψ and χ, as solutions to (3), where $\boldsymbol{\psi} = (\psi_1, \psi_2)^{\mathrm{T}}$ and $\boldsymbol{\chi} = (\chi_1, \chi_2)^{\mathrm{T}}$. Further, $\boldsymbol{\psi}$ and $\boldsymbol{\chi}$ satisfy the boundary conditions expressed as

$$\begin{cases} \boldsymbol{\psi}(\xi,T) = \begin{pmatrix} 1 \\ 0 \end{pmatrix} e^{-i\xi T} & (T \to -\infty) \\ \bar{\boldsymbol{\psi}}(\xi,T) = \begin{pmatrix} 0 \\ -1 \end{pmatrix} e^{i\xi T} & (T \to -\infty) \end{cases} \tag{4}$$

$$\begin{cases} \boldsymbol{\chi}(\xi,T) = \begin{pmatrix} 0 \\ 1 \end{pmatrix} e^{i\xi T} & (T \to \infty) \\ \bar{\boldsymbol{\chi}}(\xi,T) = \begin{pmatrix} 1 \\ 0 \end{pmatrix} e^{-i\xi T} & (T \to \infty) \end{cases} \tag{5}$$

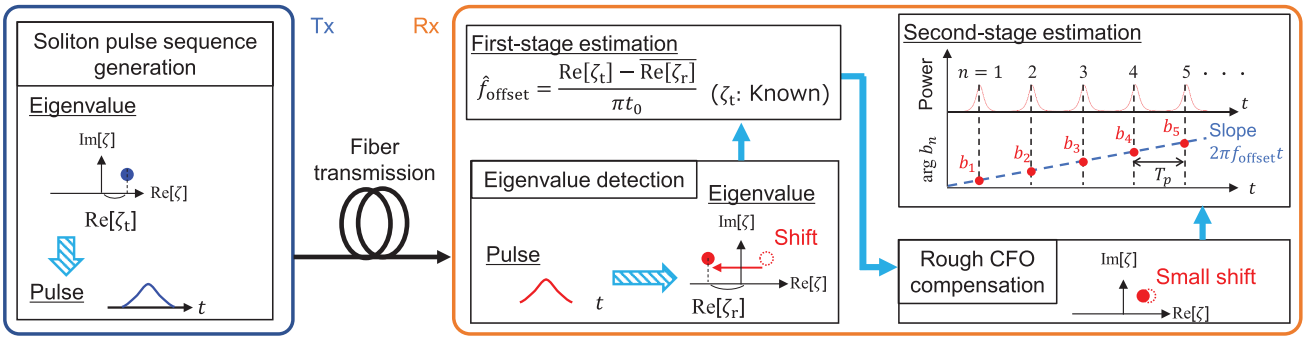

Fig. 2. IST-based CFO estimation method.

The pair of solutions, ψ and χ, gives a complete system of solutions. By introducing scattering coefficients $a(\xi)$ and $b(\xi)$,

$$\boldsymbol{\psi}(\xi, T) = a(\xi)\bar{\boldsymbol{\chi}}(\xi, T) + b(\xi)\boldsymbol{\chi}(\xi, T). \tag{6}$$

The solutions ψ and χ are analytic continuations into the upper half-plane $\text{Im}[\zeta] > 0$ ($\mathbb{C}^+$). The scattering coefficients can be obtained as

$$a(\zeta) = \lim_{T\to\infty} \psi_1(\zeta, T)e^{i\zeta T},\ b(\zeta) = \lim_{T\to\infty} \psi_2(\zeta, T)e^{-i\zeta T}. \tag{7}$$

The coefficients a and b correspond to the amplitudes of the incident and reflected waves for $T \to \infty$.

The evolution of the scattering coefficient b concerning distance Z is given by

$$b(\zeta, Z) = b(\zeta, Z = 0)e^{2i\zeta^2 Z} \tag{8}$$

The scattering coefficient b linearly evolves with distance Z of the optical fiber and can be easily compensated at a receiver.

Various multilevel modulation schemes based on IST have been proposed. Specifically, a method to realize a 2^N-ary multilevel modulation signal using on-off states of multiple eigenvalues ζ_n [4], [18], [19] and schemes to realize QPSK and 16-QAM by varying the amplitude and phase of the scattering coefficient [3] have been proposed. In such modulation schemes, coding is performed at the transmitter to assign bit sequences to patterns of eigenvalue ζ or scattering coefficient $b(\zeta)$. Then, solitons corresponding to the eigenvalue ζ and scattering parameter $b(\zeta)$ are generated, and the soliton pulse sequence is transmitted as an optical signal into the fiber. At the receiver, the eigenvalue ζ or the scattering parameter $b(\zeta)$ are detected from the complex envelope amplitude of the received soliton and decoded into a bit sequence. In such modulation schemes, the eigenvalue ζ is constant regardless of the propagation length, and the scattering parameter $b(\zeta)$ evolves linearly with the propagation length. Therefore, the modulation schemes remain unaffected by nonlinear distortions and are expected to be promising for future technology to overcome the Kerr nonlinearity limit.

B. CFO Estimation Method

The proposed CFO estimation method is illustrated in Fig. 2. The method comprises two stages: 1) an estimation based on the eigenvalue; and 2) an estimation using coefficient b. In IST-based transmission, bit data are encoded into states of the eigenvalue or b, and soliton pulses are transmitted, which are further converted using IST corresponding eigenvalue ζ and scattering coefficient b [2]. Then, a receiver detects the eigenvalue or b, which is decoded into a bit sequence.

Solutions to (3) with N discrete eigenvalues are called N-soliton solutions. In the case that a soliton pulse has one eigenvalue ζ ($N = 1$), the soliton is called a one-soliton solution, given by $\zeta = (\kappa + i\eta)/2$, where κ and η (> 0) are arbitrary real numbers. The solution to (3) is expressed as

$$u(Z, T) = \eta \text{sech}\{\eta\,(T + \kappa Z) - T_0\} \times \exp\left\{-i\left(\kappa T - \frac{\eta^2 - \kappa^2}{2} Z - \theta_0\right)\right\} \tag{9}$$

where T_0 and θ_0 are the center position and phase of the soliton peak at $Z = 0$. In (9), the phase of the soliton pulse varies with time T by $-\kappa T$. The frequency shift of the received pulse appears as a shift of the real part of the eigenvalue $\text{Re}[\zeta] = \kappa/2$. Conversely, the imaginary part of the eigenvalue $\text{Im}[\zeta] = \eta/2$ represents the amplitude and pulse width of the soliton pulse. T_0 and θ are related to the scattering coefficient b satisfying $T_0 = \log|b(\zeta, Z = 0)|$ and $\theta = \arg b(\zeta, Z = 0)$.

The relationship between the frequency shift f and the eigenvalue shift is expressed as

$$u(T)\exp(i2\pi\Delta f t_0 T) \Leftrightarrow \zeta - \pi\Delta f t_0 \tag{10}$$

where t_0 is the reference time for signal normalization, which satisfies $T = t/t_0$ for real time t. Herein, t_0 corresponds to the temporal pulse width of a 1-soliton solution that has an eigenvalue of $0.5i$.

The relationship in (10) can be applied to the case of N-soliton solutions with N eigenvalues. We assume a soliton solution with a CFO given as $\widetilde{u} = u\exp(i2\pi\Delta f t_0 T)$ in the eigenvalue (3). Moreover, the eigenfunctions with the CFO of $\widetilde{\phi}_1 = \phi_1\exp(i\pi\Delta f t_0 T)$ and $\widetilde{\phi}_2 = \phi_2\exp(-i\pi\Delta f t_0 T)$ are introduced. By substituting the solution and eigenfunctions with the CFO into (3), we obtain

$$\begin{cases} \frac{\partial\widetilde{\phi}_1}{\partial T} = -i\widetilde{\zeta}\widetilde{\phi}_1 + i\widetilde{u}\widetilde{\phi}_2 \\ \frac{\partial\widetilde{\phi}_2}{\partial T} = i\widetilde{u}^*\widetilde{\phi}_1 + i\widetilde{\zeta}\widetilde{\phi}_2 \end{cases} \tag{11}$$

where $\widetilde{\zeta} = \zeta - \pi\Delta f t_0$. Therefore, the eigenvalue $\widetilde{\zeta}$, in which only the real part is shifted by $\pi\Delta f t_0$, is obtained in the presence of the CFO.

In the first stage, the CFO is estimated by calculating the difference in the real part of the eigenvalue between the transmitted and received soliton pulses [12]. The estimated CFO $\hat{f}_{\text{offset}}$ is given by

$$\hat{f}_{\text{offset}} = \frac{\text{Re}[\zeta_{\text{t}}] - \overline{\text{Re}[\zeta_{\text{r}}]}}{\pi t_0} \tag{12}$$

where ζ_{t} and ζ_{r} are the transmitted and received eigenvalues, respectively. In a real system, CFO is estimated by using a pilot pulse with known eigenvalues and referring only to the eigenvalues of the received pulses. Alternatively, when the real part of the eigenvalues of the transmitted pulses are set to zero ($\text{Re}[\zeta_{\text{t}}] = 0$), and only the imaginary part of the eigenvalues or the scattering coefficients are varied, CFO can be estimated without using pilot pulses. Eigenvalue-based estimations treat a wide range of CFO, such as ± 5 GHz; however, the estimation accuracy is limited by the conditions of the transceiver and soliton pulse.

For this study, we employ the coefficient b-based estimation as a second stage after a rough CFO compensation using the eigenvalue-based method. As shown in Fig. 2, the scattering coefficient b is detected for each soliton pulse at the second stage. The phase of the soliton component corresponds to the argument of the scattering coefficient b. The estimated CFO at the second stage is given by

$$\hat{f}_{\text{offset}} = \frac{1}{2\pi T_p (N_p - 1)} \sum_{n=1}^{N_p} (\arg b_n - \arg b_{n-1}) \tag{13}$$

where T_p and N_p represent the pulse period and the number of pulses, respectively. A phase unwrapping process is required when a transition of arg b is traced. Therefore, an applicable CFO range for the b-based estimation is $|\hat{f}_{\text{offset}}| < 1/(2T_p)$. Combining the b-based method with the first stage estimation, we achieve a wide range and high-accuracy CFO estimation.

The proposed method can be applied to optical fiber transmission systems in two ways. One is an approach using pilot pulses inserted periodically at the beginning of the frame. In this case, the proposed method can be used as a standalone alternative CFO estimation method for NFT-based transmission systems and any optical fiber transmission systems. The other approach is the pilotless CFO estimation for NFT-based transmission systems. In the b-modulation using eigenvalues on the imaginary axis ($\text{Re}\,[\zeta_{\text{t}}] = 0$), it is possible to estimate the CFO from the signal pulses without the pilot pulses. When $\text{Re}[\zeta_{\text{t}}]$ is known for all eigenvalues in (12), the eigenvalue-based estimation at the first stage can be performed without the pilot pulses. Moreover, the scattering coefficient b-based estimation at the second stage can be extended to apply to the b-modulated signal. For example, the slope of the argument of b, which corresponds to the CFO in (13), can be estimated using the M th power method [20] for the b-modulated signal of M-ary PSK. Note that the applicable CFO range for the b-based method is limited to $|\hat{f}_{\text{offset}}| < 1/(2MT_p)$ when the Mth power method is used.

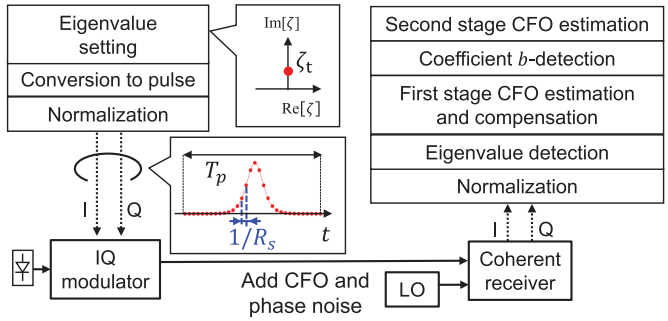

Fig. 3. Simulation model.

Compared with the periodogram-based method, the proposed method can potentially reduce the required number of pulses (symbols) and computational complexity. The details of the simulation results, including the feasibility of the pilotless estimation and the computational complexity, are discussed in Section III-B.

III. Numerical Simulations

A. Simulation Model

The characteristics of the proposed CFO estimation method were investigated through simulations. The simulation model is shown in Fig. 3. CFO estimation was performed using a fundamental soliton pulse with an eigenvalue of $\zeta = 0.3i$ ($\text{Re}[\zeta] = 0$) for the standard condition. The scattering coefficient was set to a constant value of $1i$. At the transmitter, a soliton pulse was generated from the eigenvalue and coefficient b, which was then transmitted as an optical pulse train using an IQ modulator. Optical pulses were received by a coherent receiver for the back-to-back configuration. CFO and phase noise were added to the received pulse. The linewidth of the laser was set to 1 kHz, which induced the phase noise assuming a Wiener process model [21]. Eigenvalues were detected from the received pulses using the Fourier collocation method [22], [23]. The Forward–Backward method [24] was used to detect scattering coefficient b. At the receiver, CFO was estimated using both methods: the eigenvalue-based [12] and the proposed method. We used 32 pulses ($N_p = 32$) for each estimation. The absolute value of the difference between the estimated and actual CFO was defined as the estimation error for evaluating the estimation accuracy. The estimation accuracy was evaluated depending on the pulse period T_p and the number of sampling points per pulse N_s (sampling rate $R_s = N_s/T_p$). Moreover, the estimation performance was observed while varying the number of pulses and eigenvalue from the standard condition. Additionally, CFO estimation was performed using a two-soliton solution (having two eigenvalues) with the eigenvalues of $\{\zeta_1, \zeta_2\} = \{0.3i, 0.15i\}$. In the simulation of the two-soliton solutions, the combination of coefficient b was varied. The reference time t_0 was set to 200ps.

B. Simulation Results

The estimation error for $T_p = 3.2$ ns and $N_s = 64$ ($R_s = 20$ GSa/s), while depending on the CFO value, is shown in Fig. 4.

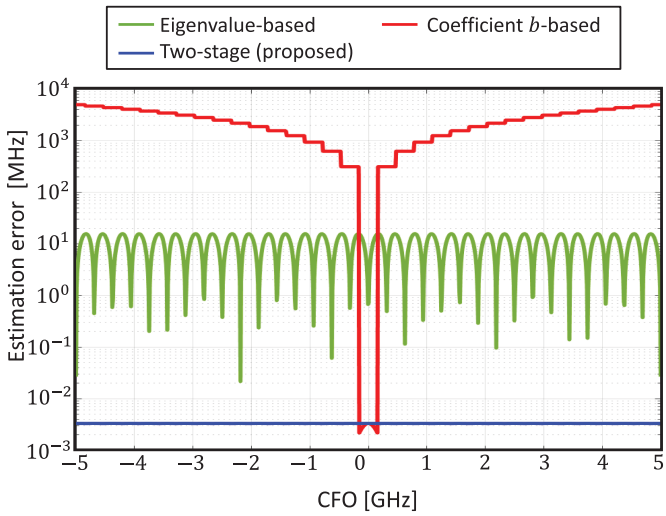

Fig. 4. CFO dependence of estimation error.

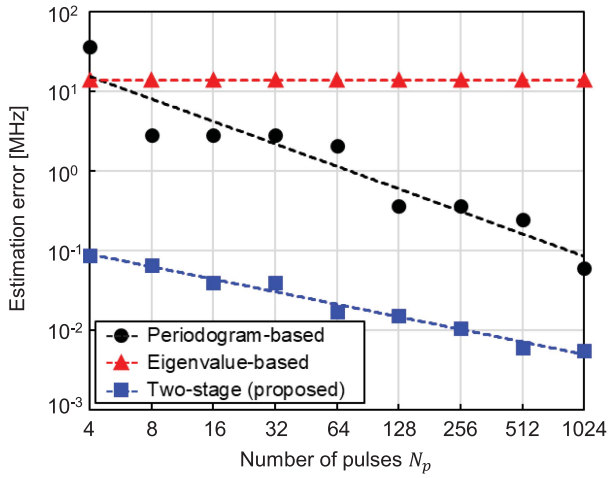

Fig. 5. Number of pulse (N_p) dependence of estimation error.

The estimation error for the eigenvalue-based method demonstrated a change with the period of the fast Fourier transform (FFT) ($1/T_p = 312.5$ MHz) because the Fourier collocation method was used for eigenvalue detection. In the Fourier collocation method, the eigenvalue problem of (3) was solved in the frequency domain to obtain the eigenvalue [22], [23]. The frequency grid was discrete because the time window size was set to a finite value of $T_p = 3.2$ ns in the simulation, which corresponded with the FFT period. Therefore, the accuracy of the eigenvalue detection depended on the frequency grid resolution ($1/T_p = 312.5$ MHz) and the CFO value. The maximum estimation error was approximately 10 MHz. The coefficient b-based method achieved a fine estimation error below 10 kHz in the CFO range from -156.25 to 156.25 MHz, corresponding to $\pm 1/(2T_p)$. However, the estimation method did not work for $|\text{CFO}| > 1/(2T_p)$. Contrarily, the proposed two-stage method achieved a consistently fine estimation with an error below 10 kHz over CFO of ± 5 GHz.

The estimation error for $T_p = 3.2$ ns and $N_s = 64$ ($R_s = 20$ GSa/s), while varying the number of pulses (N_p) from 2 to 1024, is shown in Fig. 5. The CFO was set to a fixed value of 119.995 MHz. For comparison, estimation errors were calculated when using the periodogram-based frequency domain estimation method [8], the eigenvalue-based estimation method, and the proposed two-stage estimation method. In the case of frequency-domain estimation, the frequency resolution improved with the number of pulses. Thus, the estimation accuracy improved; however, a high estimation accuracy required a large number of pulses and a long estimation time. In the case of eigenvalue-based estimation, the estimation accuracy was independent of the number of pulses and was recorded as 13 MHz. The estimation accuracy of the eigenvalue-based method was limited by the pulse period T_p. When T_p was not sufficiently long, such as 3.2ns, the tail of the soliton pulse was cut, resulting in the eigenvalue detection error [12]. By contrast, the proposed two-stage method achieved higher estimation accuracy with fewer pulses than frequency-domain estimation, while estimation accuracy of less than 10 kHz was obtained with $N_p \geqq 512$. The accuracy of the frequency-domain estimation depended on the frequency resolution of the FFT, namely the total time window size ($T_p \times N_p$). Conversely, the second-stage estimation of the proposed method monitored the phase of the soliton components and estimated the CFO from the slope of the phase change, achieving a fine estimation accuracy.

The contour chart of the estimation error when using the eigenvalue-based and proposed methods, on varying the pulse period T_p and sampling points N_s (sampling rate R_s), is shown in Fig. 6. The CFO was set to a fixed value of 119.995 MHz. The estimation error was measured as the average of the absolute error values after 10 estimation iterations. For the eigenvalue-based method, the estimation error increased when T_p or R_s were small because the eigenvalue was not detected precisely when the edges of the soliton pulse and spectrum were eliminated under the limited conditions. When T_p and R_s were sufficiently large, such as $T_p = 6.4$ ns and $R_s = 20$ GSa/s, the estimation error was approximately 100 kHz. For the proposed method, the estimation error significantly increased when $R_s < 2.5$ GSa/s because the first stage estimation in the eigenvalue domain did not work well. When the sampling rate was 5 GSa/s or more, a fine estimation below 100 kHz was achieved even for $|\text{CFO}| > 1/(2T_p)$, with a large T_p. For $T_p = 25.6$ ns and $R_s = 10$ GSa/s, an estimation accuracy below 10 kHz was obtained. Thus, the proposed method achieved more precise and stable estimation accuracy for a wide range of pulse period T_p and sampling rate R_s.

The estimation error for $R_s = 20$ GSa/s while varying the eigenvalue and T_p is shown in Fig. 7. The estimation error for the eigenvalue-based CFO estimation decreased as pulse period increased. Since pulse width varied with eigenvalue, the estimation accuracy was affected by both the window size and eigenvalue. With sufficient pulse period, the estimation error was independent of eigenvalues, and estimation accuracy below 100 kHz was obtained when $T_p \geqq 25.6$ ns. The two-stage estimation method allowed for more accurate estimations, independent of eigenvalues for short pulse periods, and an estimation

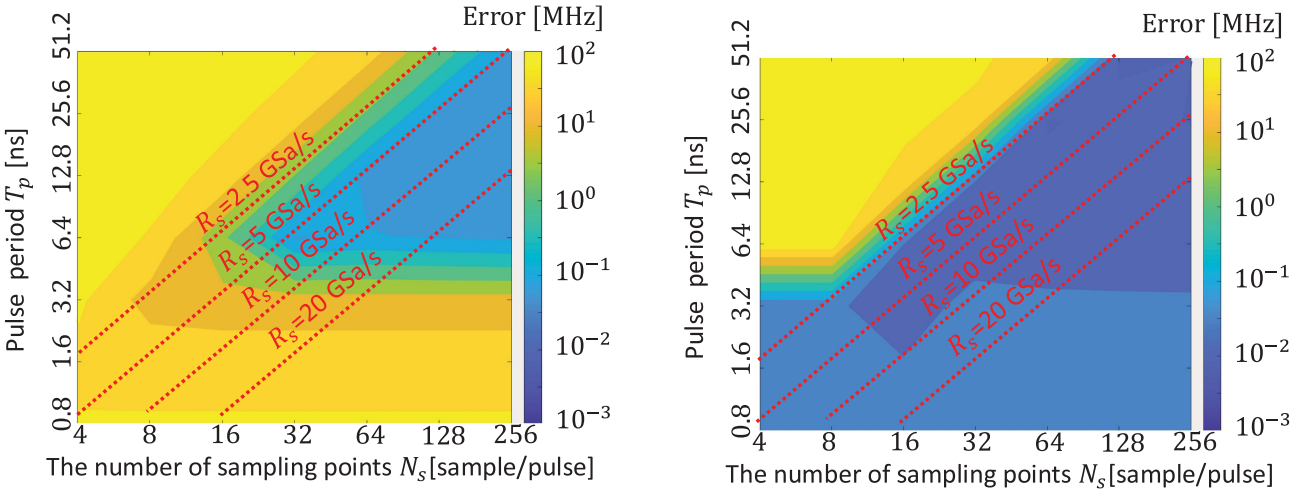

(a) Eigenvalue-based CFO estimation (b) Two-stage CFO estimation

Fig. 6. Contour chart of estimation error.

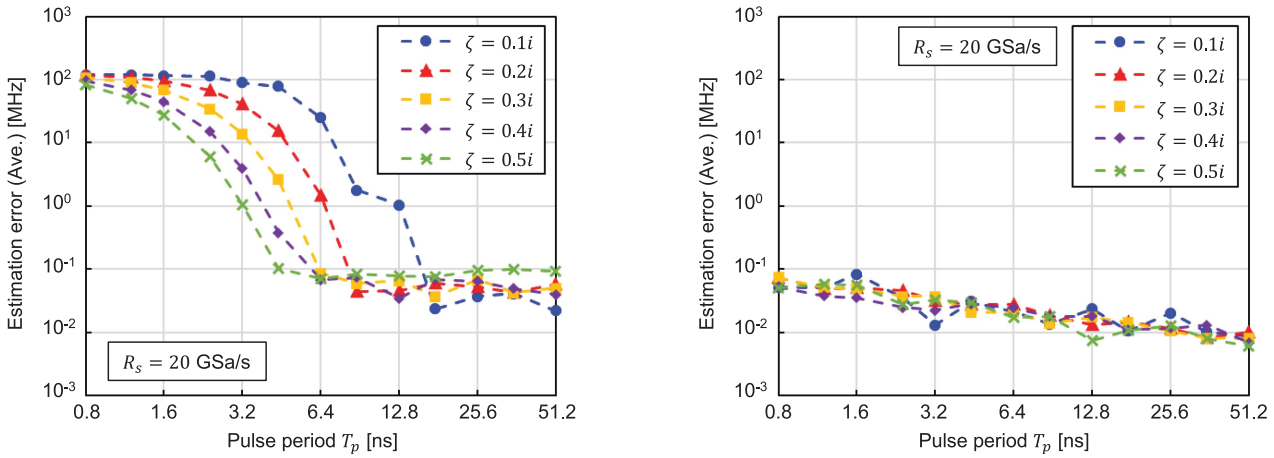

(a) Eigenvalue-based CFO estimation (b) Two-stage CFO estimation

Fig. 7. Eigenvalue dependence of the CFO estimation error.

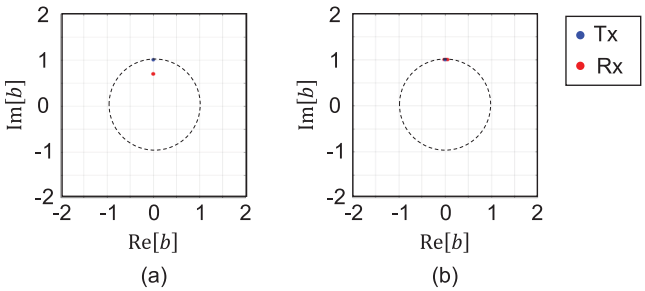

Fig. 8. Constellation diagrams of the scattering coefficient b for T_p of (a) 0.8 ns and (b) 25.6 ns.

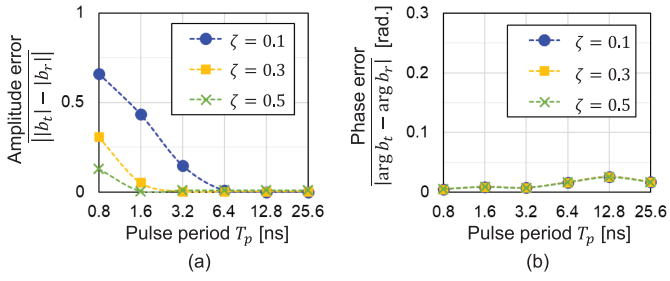

Fig. 9. Errors of the amplitude and phase of the detected b varying the pulse period T_p for various eigenvalues.

accuracy of approximately 10 kHz was obtained for $T_p = 51.2$ ns. Fig. 8 shows the constellation diagrams of the scattering coefficient b of $\zeta = 0.3i$ for $T_p = 0.8$ and 25.6ns. When the pulse period (window size) was sufficiently long, such as at 25.6ns, b was accurately detected at the receiver, as shown in Fig. 8(b). For $T_p = 0.8$ ns, although the amplitude of b was shifted, the error of the phase of b was sufficiently small, as shown in Fig. 8(a). Fig. 9 shows the errors of the amplitude and phase of the detected b, varying the pulse period T_p for various eigenvalues. The amplitude error increased as T_p decreased.

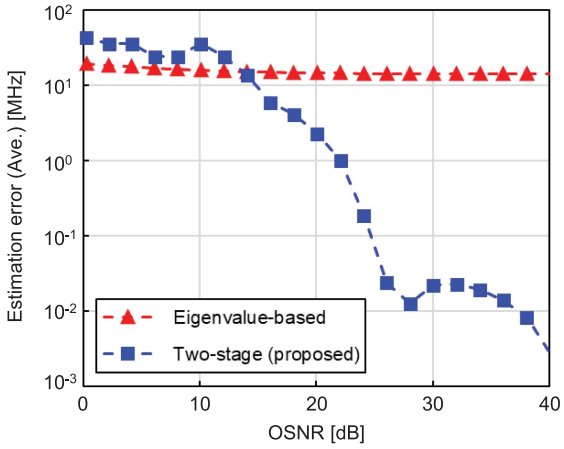

Fig. 10. OSNR dependence of the CFO estimation error.

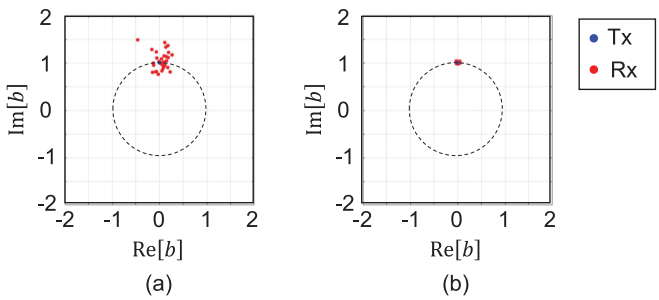

Fig. 11. Constellation diagrams of the scattering coefficient b for OSNR of (a) 0 dB and (b) 20 dB.

However, the phase error remained below 0.03 rd regardless of the eigenvalue and T_p conditions. These results indicate that the phase information of the soliton pulse was maintained even when the tail of the soliton was trimmed by the short pulse period. In the second-stage estimation of the proposed method, only the phase of b, not the amplitude of b, was used for the estimation, as described in (13). Even though the estimation at the first stage of the eigenvalue-based method was inaccurate, the second-stage estimation worked well, provided that the CFO before the second stage was within the applicable range ($|\mathrm{CFO}| > 1/(2T_p)$). Therefore, the two-stage estimation achieved a high estimation accuracy across a wide eigenvalue and T_p range.

Fig. 10 shows the estimation error for $\zeta = 0.3i$, $T_p = 3.2$ ns, and $N_s = 64$ ($R_s = 20$ GSa/s) while varying the optical signal-to-noise ratio (OSNR). We assumed that white Gaussian noise was added to the optical amplifier in the simulation. The estimation error for the eigenvalue-based method showed a constant estimation accuracy of about 10 MHz. For a low OSNR below 14 dB, the two-stage estimation reduced the estimation accuracy compared with the first-stage estimation. This is because a large noise induced a significant variation in the scattering coefficient b, which increased the estimation error. As described in the previous paragraph, a short pulse period did not significantly affect the phase of b. In contrast, as shown in Fig. 11(a), a large noise induced a significant variation in the phase of b. Because the estimation at the second stage

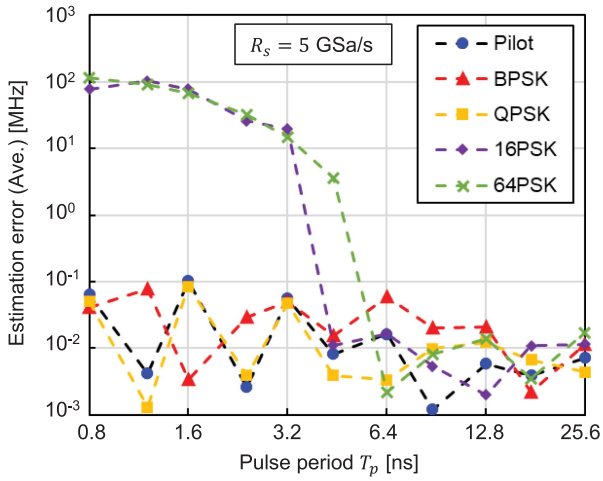

Fig. 12. Estimation error varying T_p for several modulation formats ($R_s = 5$ GSa/s).

referred to the phase of b, as described in (13), the variation in the phase of b degraded the estimation accuracy. Conversely, a clear constellation diagram of the scattering coefficient b with a slight variation in the phase was observed under a high OSNR condition, as shown in Fig. 11(b). The two-stage estimation method yielded more accurate estimates than eigenvalue-based methods for OSNR ≥ 14 dB, and a fine estimation accuracy below 30 kHz was achieved for OSNR ≥ 26 dB.

Next, we discuss the applicability of the proposed method to the modulated signal using the scattering coefficient b. In this paragraph, we describe the results of the CFO estimation using a b-modulated signal instead of a pilot pulse sequence (repeated pulse sequence). The modulation formats of BPSK, QPSK, 16 PSK, and 64 PSK were examined. The Mth power method [20] was used to treat the modulated signal similarly to the pilot pulse sequence before the second-stage CFO estimation. Fig. 12 shows the estimation error varying the pulse period T_p for several modulation formats ($R_s = 5$ Gsample/s). For the BPSK and QPSK formats, a comparable high estimation accuracy with the case using the pilot pulses was achieved even when $T_p = 0.8$ ns. This result demonstrated the feasibility of the pilotless CFO estimation without the pilot pulses. When using a QPSK of $T_p = 0.8$ ns, the symbol rate was 1.25 Gsymbol/s, where a symbol comprises two bits. This resulted in a data rate of 2.5 Gbps. The sampling rate was 5 GSa/s; therefore, the oversampling rate was 4 samples/symbol. If the proposed method can be applied while increasing the number of eigenvalues for b -modulation to two or four, the data rate can be increased to 5 or 10 Gbps. For the 16 PSK and 64 PSK formats, the estimation error reduced significantly when $T_p \leq 3.2$ ns. This is because the remaining CFO after the first-stage estimation was out of the range of the second-stage estimation. When the Mth power method was used, the acceptable CFO range of the second-stage estimation decreased to $|\hat{f}_{\mathrm{offset}}| < 1/(2MT_p)$. For example, the remaining CFO after the first stage was approximately 100 MHz for 16 PSK and $T_p = 0.8$ ns. Conversely, the applicable CFO range for $M = 16$ was approximately 40 MHz. Therefore, the

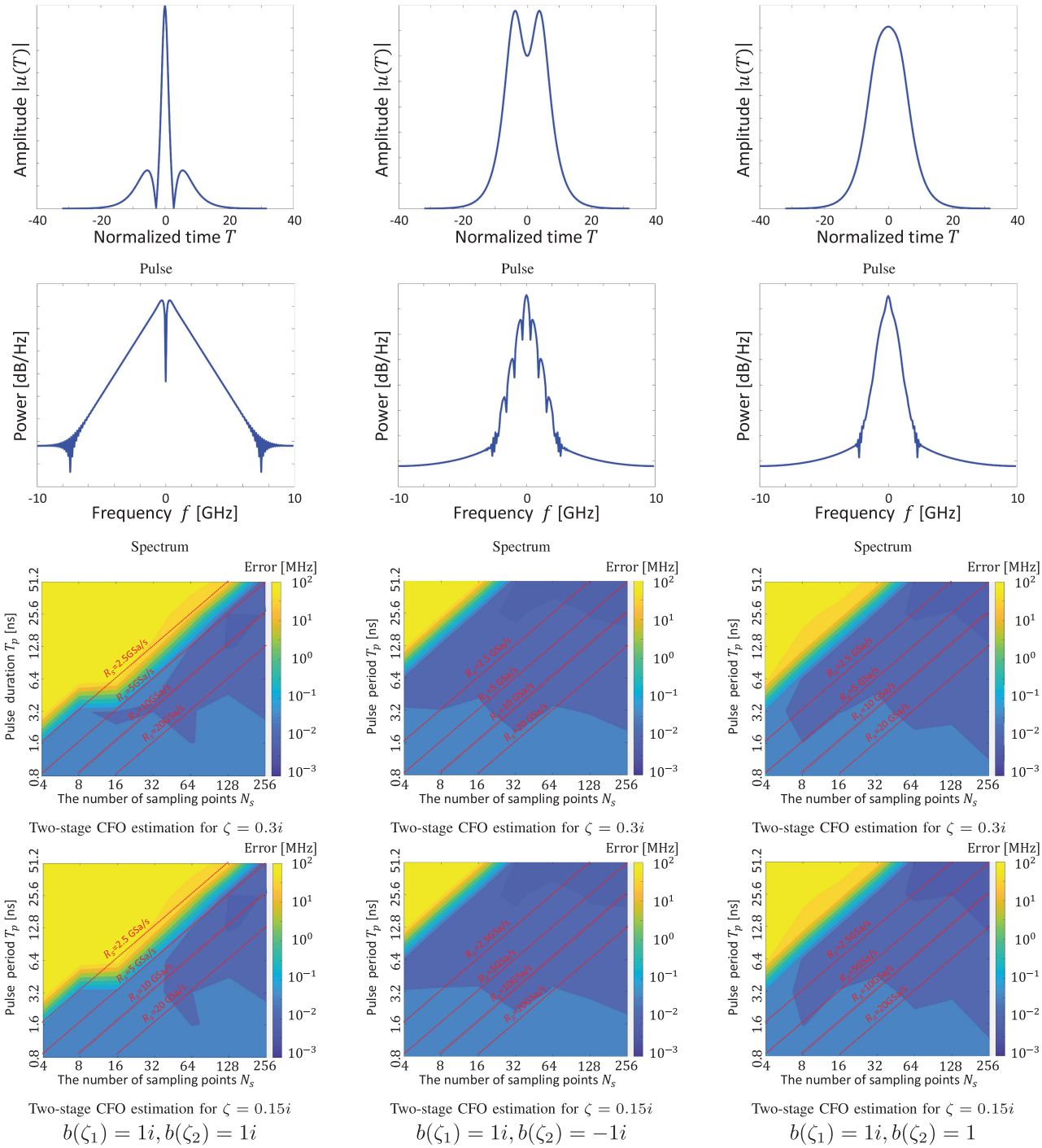

Fig. 13. Contour chart of the estimation error using two-soliton solution.

second-stage estimation did not work for $M \geq 16$. When the second-stage estimation succeeded using 64 PSK of $T_p = 6.4$ ns, the data rate was 0.9375 Gbps. Improving the estimation accuracy of the rough first-stage estimation is necessary to apply the fine second-stage estimation. Improving the first-stage estimation or combining it with other fine first-stage estimations remains a matter to be discussed further.

Furthermore, we discuss the applicability of the proposed method to 2-soliton solutions. The pulse, spectrum, and contour charts of the estimation error for the proposed method are shown in Fig. 13, which depend on the pulse period T_p and sampling points N_s(sampling rate R_s) when 2-soliton solution with eigenvalues of $0.3i$ and $0.15i$ are considered. We examined three combinational patterns of the scattering coefficient b of $(1i, 1i)$, $(1i, -1i)$, and $(1i, 1)$. In the proposed two-stage method, almost the same contour charts were observed for both eigenvalues. When T_p and R_s were sufficiently large, such as $T_p = 6.4$ ns and $R_s = 20$ GSa/s, the estimation error was approximately 10 kHz for both eigenvalues. The difference in estimation error due to the scattering coefficient b was observed in the low baud

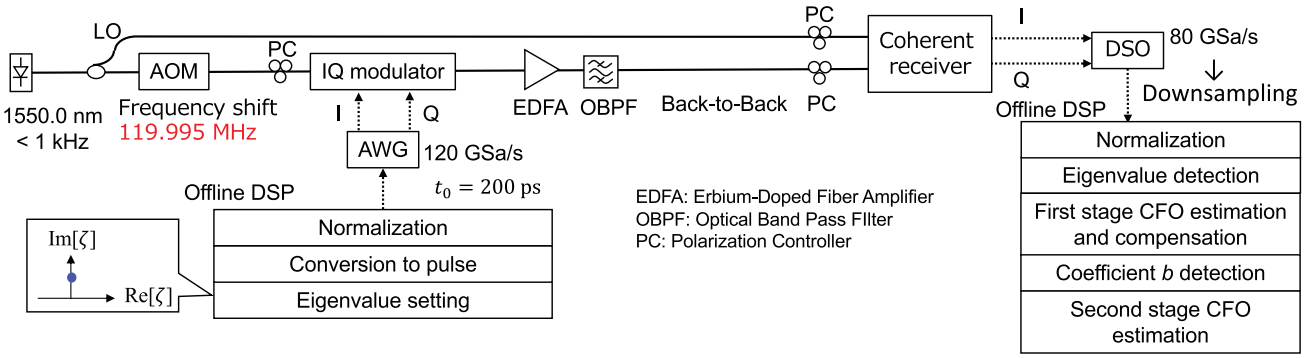

Fig. 14. Experimental setup.

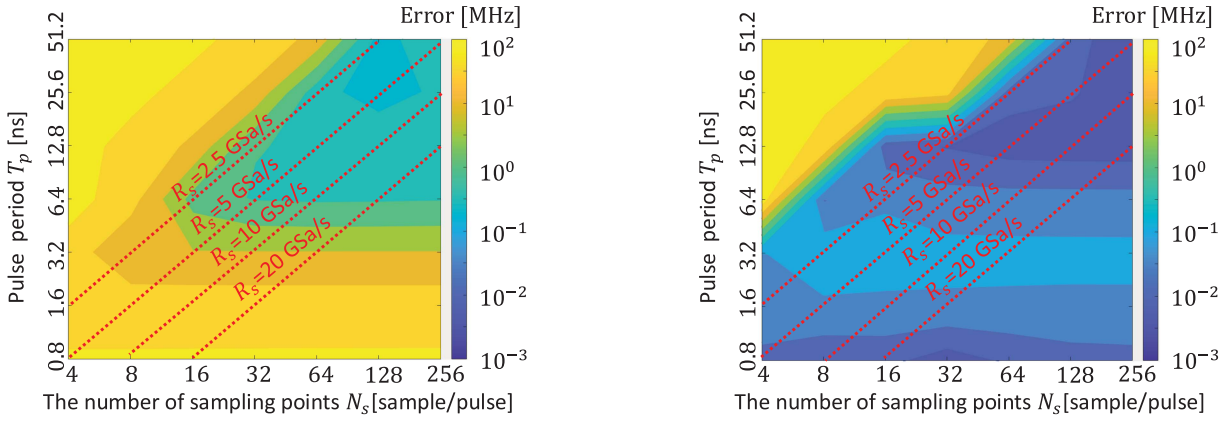

Fig. 15. Contour chart of the estimation error obtained in the experiments.

rate region because different combinations of scattering coefficients b exhibited different waveforms and spectra, and different baud rates were required to correctly recover the waveforms. However, the proposed two-stage method estimated CFO for waveforms with multiple peak spectra that were not easy to estimate in the frequency domain.

Finally, we discuss the computational complexity. The proposed CFO estimation requires the number of flops of $\mathcal{O}(N_p N_s^3)$ for eigenvalue detection using the Fourier collocation method, which is significantly larger than $\mathcal{O}(N_p N_s)$ for the detection of the scattering coefficient b for a discrete eigenvalue [2], [24] Conversely, the periodogram-based estimation in the frequency domain requires $\mathcal{O}(N_p N_s \log_2(N_p N_s))$ flops for the FFT. The number of pulses N_p required to achieve an estimation accuracy of approximately 0.1 MHz were 2 and 1024 for the proposed and periodogram-based methods, respectively, as shown in Fig. 5. The proposed method has the advantage of requiring fewer numbers of pulses and total sampling points than the periodogram-based method. For the number of sampling points per pulse of $N_s = 64$ in Fig. 5, the total computational complexity of the proposed method was slightly lower than that of the periodogram-based method. Although the computational complexity of the periodogram method is determined by the total time window size $T_p N_p N_s$, the proposed method can reduce the computational complexity by decreasing N_s . For example, as shown in Fig. 6(b), the proposed method achieved a fine estimation accuracy below 0.1 MHz under the condition of $N_s = 4$ and $N_p = 64$. In this case, $N_p N_s^3$ and $N_p N_s$ are significantly smaller than $N_p N_s \log_2(N_p N_s))$ for $N_p N_s = 1024 \times 64$. The proposed method can significantly reduce the computational complexity depending on the conditions and accuracy of the target estimation. In addition, several algorithms have been studied to reduce the computation complexity and time for eigenvalue detection [2], [25].

IV. Experiments

A. Experimental Setup

We investigated the CFO estimation accuracy of the proposed method through experiments for back-to-back configuration. The experimental setup is shown in Fig. 14. A shared lightwave source with linewidth $<$ 1 kHz was used for the signal light and LO to provide a static CFO. An acoustic optical modulator (AOM) introduced a static frequency shift of 119.995 MHz on the signal measured using the periodogram method with a long measurement time. An optical soliton pulse was generated using an arbitrary waveform generator (AWG) and an IQ modulator. A coherent receiver received the optical soliton pulse, and analog to digital (A/D) conversion was performed using a digital storage oscilloscope (DSO) at 80 GSa/s. The CFO was estimated

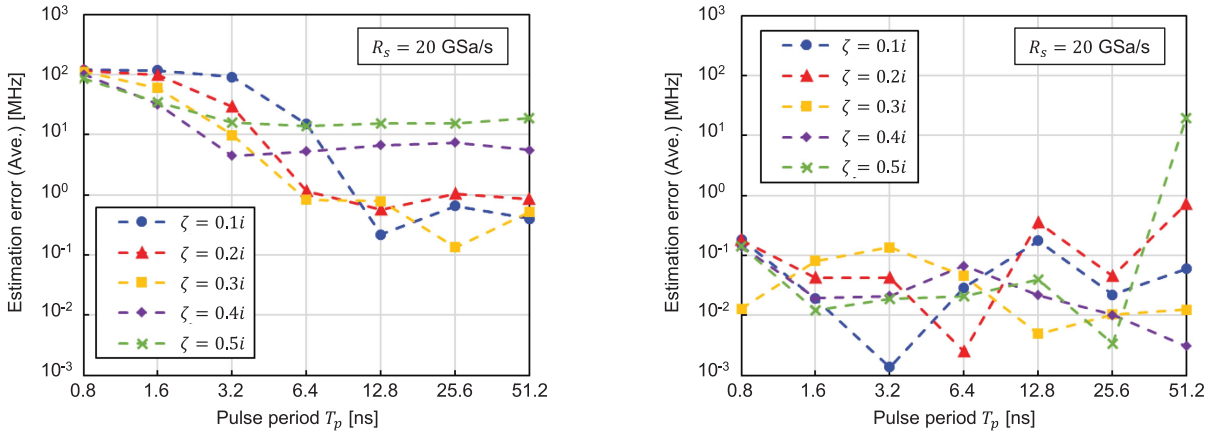

(a) Eigenvalue-based CFO estimation

(b) Two-stage CFO estimation (proposed)

Fig. 16. Eigenvalue dependence of the CFO estimation error in the experiments.

using the eigenvalue-based and the proposed two-stage methods. Other parameters and digital signal processing (DSP) results for pulse generation and CFO estimation were identical to those obtained in the simulation. The estimation accuracy was evaluated varying the pulse period T_p and sampling points N_s (sampling rate R_s).

B. Experimental Results

The contour chart of the estimation error is shown in Fig. 15. Compared with the simulation results (Fig. 6), comparable estimation accuracy results were obtained with similar trends and kilo-Hertz-order precision over a wider area in the experiments. For the eigenvalue-based method, the estimation error was approximately 1 MHz for $T_p > 3.2$ ns and $R_s > 2.5$ GSa/s. On using the proposed method, a better estimation accuracy below 10 kHz was achieved under the conditions of $T_p > 12.8$ ns and $R_s > 5$ GSa/s.

The estimation error for $R_s = 20$ GSa/s while varying the eigenvalue and T_p is shown in Fig. 16. Similar to the simulation (Fig. 7), the eigenvalue-based CFO estimation method showed a smaller estimation error for a larger pulse period. In the two-stage CFO estimation method, an estimation accuracy of less than 1 MHz was obtained in almost all regions. At $\zeta = 0.5i$ and $T_p = 51.2$ ns, the estimation accuracy did not improve to approximately 15 MHz because the applicable CFO range at the second stage was approximately 10 MHz or less, and the first-stage eigenvalue-based CFO estimation could not bring the estimation accuracy within that range. In particular, when T_p was large, the detection accuracy of the scattering coefficient b deteriorated because the edge of the soliton waveform was noisy; therefore, the estimation accuracy was unstable.

V. Conclusion

This paper proposes a novel CFO estimation method that combines eigenvalue-based and scattering coefficient b-based methods. The feasibility and characteristics of the proposed two-stage CFO estimation method are investigated through numerical simulations and experiments. The two-stage CFO estimation method achieves an estimation accuracy of less than 10 kHz error in numerical simulations under the condition of pulse period $T_p = 25.6$ ns and sampling rate $R_s = 10$ GSa/s. Furthermore, the dependencies of noise and eigenvalue are investigated. A fine estimation accuracy below 30 kHz is recorded for OSNR ≥ 26 dB. Additionally, the proposed method is validated even for two-soliton solutions with a multipeak spectrum. In the experimental demonstration, estimation accuracy below 10 kHz is attained under the conditions of $T_p > 12.8$ ns and $R_s > 5$ GSa/s, and the two-stage estimation method achieves better estimation accuracy than the eigenvalue-based method.

Although the feasibility of the proposed method in the B-to-B configuration was demonstrated by focusing on its basic characteristics in this study, it is applicable to fiber transmission systems, provided that the NLSE (2) is satisfied. However, several factors perturb the NLSE in IST-based transmission systems, such as fiber loss, optical amplifier noise, third-order dispersion, and nonlinearity of transceivers, which may limit the applicable range of the proposed method. A future study will aim to prove the applicability of the proposed method to fiber transmission and digital signal processing with demodulation via experimental demonstration.

References

[1] M. J. Ablowitz and H. Segur, *Solitons and the Inverse Scattering Transform*. Philadelphia, PA, USA: SIAM, 1981.

[2] S. K. Turitsyn et al., "Nonlinear Fourier transform for optical data processing and transmission: Advances and perspectives," *OSA Optica*, vol. 4, no. 3, pp. 307–322, Mar. 2017.

[3] T. Gui, T. H. Chan, C. Lu, A. P. T. Lau, and P.-K. A. Wai, "Alternative decoding methods for optical communications based on nonlinear Fourier transform," *IEEE/OSA J. Lightw. Technol.*, vol. 35, no. 9, pp. 1542–1550, May 2017.

[4] H. Takeuchi, K. Mishina, Y. Terashi, D. Hisano, Y. Yoshida, and A. Maruta, "Eigenvalue-domain neural network receiver for 4096-ary Eigenvalue-modulated signal," in *Proc. Opt. Fiber Commun. Conf. Exhib.*, San Diego, CA, USA, Mar. 2022, paper Th3F.3.

[5] L. Li, Z. Tao, S. Oda, T. Hoshida, and J. C. Rasmussen, "Wide-range, accurate and simple digital frequency offset compensator for optical coherent receivers," in *Proc. OFC/NFOEC Conf. Opt. Fiber Commun./Nat. Fiber Optic Engineers Conf.*, San Diego, CA, USA, Mar. 2008, paper OWT4.

[6] Optical Internetworking Forum, "Integrable tunable laser Assembly MSA," OIF-ITLA-01.2, Jun. 2008.

[7] Optical Internetworking Forum, "Micro integrable tunable laser assembly," OIF-MicroITLA-01.0, Sep. 2011.
[8] T. Nakagawa et al., "Non-data-aided wide-range frequency offset estimator for QAM optical coherent receivers," in *Proc. Opt. Fiber Commun. Conf. Expo., Nat. Fiber Optic Engineers Conf.*, Los Angeles, CA, USA, Mar. 2011, paper OMJ1.p.
[9] M. Selmi, Y. Jaouen, and P. Ciblat, "Accurate digital frequency offset estimator for coherent PolMux QAM transmission systems," in *Proc. 35th Eur. Conf. Opt. Commun.*, Vienna, Austria, Sep. 2009, paper P3.08.
[10] Y. Cao, S. Yu, Y. Chen, Y. Gao, W. Gu, and Y. Ji, "Modified frequency and phase estimation for M-QAM optical coherent detection," in *Proc. 36th Eur. Conf. Exhib. Opt. Commun.*, Trino, Italy, Sep. 2010, paper We.7.A.1.
[11] D. Zhao, L. Xi, X. Tang, W. Zhang, Y. Qiao, and X. Zhang, "Digital pilot aided carrier frequency offset estimation for coherent optical transmission system," *OSA Opt. Exp.*, vol. 23, no. 19, pp. 24822–24832, Sep. 2015.
[12] T. Maeda, D. Hisano, Y. Yoshida, A. Maruta, and K. Mishina, "Carrier frequency offset estimation in the eigenvalue domain," *IEEE/Optica J. Lightw. Technol.*, vol. 41, no. 21, pp. 6691–6699, Nov. 2023.
[13] Z. Zheng, X. Zhang, R. Yu, L. Xi, and X. Zhang, "Frequency offset estimation for nonlinear frequency division multiplexing with discrete spectrum modulation," *OSA Opt. Exp.*, vol. 27, no. 20, pp. 28223–28238, Sep. 2019.
[14] T. Chino, T. Motomura, A. Maruta, and K. Mishina, "Double-stage carrier frequency offset estimation using the eigenvalue and scattering coefficient b in the nonlinear fourier transform," in *Proc. Opt. Fiber Commun. Conf. Exhib.*, San Diego, CA, USA, Mar. 2024, paper M4F.3.
[15] J. He et al., "Blind frequency offset estimation method based on a minimum phase correction error for a full spectrum modulated NFDM system," *Optica Opt. Lett.*, vol. 49, no. 9, pp. 2313–2316, May 2024.
[16] G. Agrawal, *Nonlinear Fiber Optics*, 5th Ed., Cambridge, MA, USA: Academic Press, 2012.
[17] A. Hasegawa and Y. Kodama, "Guiding-center soliton in optical fibers," *OSA Opt. Lett.*, vol. 15, no. 24, pp. 1443–1445, Dec. 1990.
[18] S. Hari, M. I. Yousefi, and F. R. Kschischang, "Multieigenvalue communication," *IEEE/OSA J. Lightw. Technol.*, vol. 34, no. 13, pp. 3110–3117, Jul. 2016.
[19] T. Kodama, K. Mishina, Y. Yoshida, D. Hisano, and A. Maruta, "Transmission of hypermultilevel eigenvalue-modulated signals using arbitrary optical multi-eigenvalues," *Opt. Commun.*, vol. 546, Nov. 2023, Art. no. 129748.
[20] A. Leven, N. Kaneda, U.-V. Koc, and Y.-K. Chen, "Frequency estimation in intradyne reception," *IEEE Photon. Technol. Lett.*, vol. 19, no. 6, pp. 366–368, Mar. 2007.
[21] E. Ip and J. M. Kahn, "Feedforward carrier recovery for coherent optical communications," *IEEE/OSA J. Lightw. Technol.*, vol. 25, no. 9, pp. 2675–2692, Sep. 2007.
[22] H. Terauchi and A. Maurta, "Eigenvalue modulated optical transmission system based on digital coherent technology," in *Proc. 18th OptoElectronics Commun. Conf. Held Jointly With Int. Conf. Photon. Switching*, Kyoto, Japan, Jul. 2013, paper WR2-5.
[23] A. Maruta, Y. Matsuda, H. Terauchi, and A. Toyota, "Digital coherent technology-based eigenvalue modulated optical fiber transmission system," in *Odyssey of Light in Nonlinear Optical Fibers: Theory and Applications*, K. Porsezian and R. Ganapathy, Eds. Boca Raton, FL, USA: CRC Press, 2015, Ch. 19, pp. 491–505.
[24] V. Aref, "Control and detection of discrete spectral amplitudes in nonlinear Fourier spectrum," May 2016, *arXiv:1605.06328*.
[25] Y. Terashi, D. Hisano, K. Mishina, Y. Yoshida, and A. Maruta, "Multieigenvalue demodulation using complex moment-based eigensolver and neural network," *IEEE/Optica J. Lightw. Technol.*, vol. 41, no. 14, pp. 4713–4724, Jul. 2023.

Taisuke Chino received the B.E. and M.E degrees in electrical, electronic, and infocommunication engineering from Osaka University, Osaka, Japan, in 2023 and 2025, respectively. He is currently with the Mitsubishi Electric Corporation, Japan.

Takumi Motomura (Graduate Student Member, IEEE) received the B.S., and M.S. degrees in 2020 and 2022, respectively. He is currently working toward the Ph.D. degree from the Graduate School of Engineering, Osaka University, Osaka, Japan,. His research interests include optical fiber communication systems and nonlinear fiber optics and its applications. He is a Member of the IEICE, Japan.

Takaya Maeda received the B.E. and M.E degrees in electrical, electronic, and infocommunication engineering from Osaka University, Osaka, Japan, in 2021 and 2023, respectively. He is currently with NEC Corporation, Japan.

Akihiro Maruta (Member, IEEE) received the B.E., M.E., and Ph.D. degrees in communication engineering from Osaka University, Osaka, Japan in 1988, 1990, and 1993, respectively. He joined the Department of Communications Engineering, Osaka University, in 1993. Since 2016, he has been a Professor with the Department of Information and Communication Technology, Osaka University. His research interests include optical fiber communication systems and all-optical signal processing. He is a Member of IEEE Photonics Society and Optical Society of America (OSA), and Senior Member of IEICE, Japan.

Ken Mishina (Member, IEEE) received the B.E., M.E., and Ph.D. degrees in electrical, electronic, and information engineering from Osaka University, Osaka, Japan, in 2005, 2007, and 2012, respectively. In 2007, he joined Shimadzu Corporation, Kyoto, Japan. Since 2018, he has been an Associate Professor with the Department of Information and Communication Technology, Division of Electrical, Electronic, and Information Engineering, Graduate School of Engineering, Osaka University. His research interests include optical fiber communication systems, all-optical signal processing and photovoltaics. He is a member of IEEE Photonics Society and IEICE, Japan.